
Comparison of point cloud densification from multi-view stereo and 3D Gaussian splatting in industrial photogrammetry

Mingda Harvey Yang, Mohammed A Isa, Adam Thompson, David T Branson III, Samanta Piano

Manufacturing Metrology Team

Faculty of Engineering, Advanced Manufacturing Building, University of Nottingham Jubilee Campus, Nottingham, NG8 1BB, UK

* Corresponding Author: samanta.piano@nottingham.ac.uk

Abstract:

Photogrammetry is increasingly popular in the modern manufacturing industry, for performing non-contact fast optical measurements of manufactured components. During photogrammetry, the goal is to obtain accurate three-dimensional reconstructions of a measurand that include information about surface form and dimensions. Using multiple two-dimensional observations of a measurand, a 3D reconstruction of the measurand can be constructed algorithmically. The main objective of this research is to compare the outcomes of the 3D reconstruction dense point cloud obtained by 3D Gaussian splatting (3DGS) to the general multi-view stereo (MVS) method. Using the same set of 2D images of the measurand as the input to the measurement pipelines of the two aforementioned methods, we obtained the full position and orientation (i.e. the extrinsic parameters) of the camera in a world coordinate system by calibrating the camera's pose for each image taken. The proposed study involves the introduction of a camera extrinsic parameter estimation step for each of the methods to obtain a point cloud that is reconstructed in the actual physical size of the measurand. The geometric dimensions and surface form details of the measurand were also measured with fringe projection profilometry (FPP) techniques using a commercial instrument GOM ATOS, presented here as the ground truth measurement to compare the scale-calibrated point clouds obtained by each of the methods above for the accuracy evaluation of the measurements.

Keywords : Photogrammetry, 3D reconstruction, 3D Gaussian splatting, scale calibration

1. Introduction

Photogrammetry is a measurement method capable of measuring and analysing the geometry of complex industrial components and systems using high-precision photographic techniques. This technique is widely used in manufacturing, engineering and construction, aerospace and other fields, especially where non-contact, high-precision measurements are required [1]. At the core of industrial photogrammetry lies the use of high-resolution cameras to capture images of objects and the use of computer vision and optical measurement principles to analyse these images [2]. By using visual features on the surface of the object, analysing the geometric properties and relationships between multiple images, photogrammetry is able to accurately reconstruct the position, size, shape and other geometric details of the object [2].

The process of photogrammetry can reconstruct three-dimensional (3D) geometries from two-dimensional (2D) images through a process that includes camera calibration, image acquisition, feature extraction, image matching and camera pose estimation from the matched feature points. Matched image features are used to obtain sparse point cloud

through a structure-from-motion (SfM) pipeline, where camera parameters and the 3D point cloud positions are optimised by minimising reprojection error using bundle adjustment. Finally, a densification process, such as MVS, is utilized to generate detailed depth map for each image to obtain dense point cloud [3].

Another method that can be used for generating dense point clouds is 3D Gaussian splatting (3DGS), a technique used to render realistic 3D scenes. Unlike traditional point cloud rendering, 3DGS works by representing each point as a Gaussian distribution. By modelling the volume and density of objects, 3DGS enables smooth and continuous rendering [4,5].

In contrast to other fields like oblique photography and aerial photogrammetry, photogrammetry in metrology field requires the consideration of accurate dimensional information. In the 3D reconstruction process, point cloud data and image data are unit-independent, which makes point clouds typically constructed on an arbitrary scale that requires adjustment. Scale calibration allows the conversion of photogrammetry data into actual physical units, making the 3D model generated from image data to be accurate in both shape and size, thus making the measurements meaningful [1]. In order to

ensure the scale and size of the reconstructed model, an object of known size is often placed in the scene for reconstruction. Common standard objects include checkerboard calibration plates, rulers, cubes or spheres. The scale of the model is adjusted by measuring the size of the known object in the reconstructed model and calculating the scale factor between the actual size and the reconstructed size. This method requires the standard object to have sufficient visual features in the scene so that it can be clearly identified and matched in the image.

To compare with the existing method of place a standard object in the scenes for reconstruction, this work investigates an automatically scale adjustment of dense point clouds generated by 3DGS and MVS, making it possible to compare and analyse results with the ground truth measurement from an industrial fringe projection profilometry (FPP) instrument.

2. Methodology

In this section the workflow for the whole photogrammetry measurement is presented. The measurand is a stepped sample made of Ti6Al4V, produced by the laser powder bed fusion (LPBF) process. The nominal dimension of the sample is 50 mm x 50 mm x 10 mm.

2.1 Experimental equipment

All image data involved in this work were obtained from a close-range photogrammetry system [6] (fig.1). A monocular Canon EOS 1300D DSLR camera is mounted in the photogrammetry system for image acquisition, the captured images were taken with the resolution of 5160×3456 corresponding with vertical and horizontal dimensions, 53 mm focal length and ISO 400 setting [6]. A motor-driven rotational stage is placed in the field-of-view the camera where the rotary axis, run-out and axial wobble of this rotational stage have been estimated [7]. The measured object (measurand) is placed on this rotational stage during the measurement process. For the image acquisition step, the camera takes one image for every six degrees stage rotation to capture a total of 60 images that cover the surface of the measurand. The images are acquired in a well-lit non-changing laboratory setting, thus reducing the uncertainty that may be caused by external factors. In addition, the experiment was carried out in a temperature-controlled laboratory at 20 ± 1 °C to ensure consistency of the measurement process.

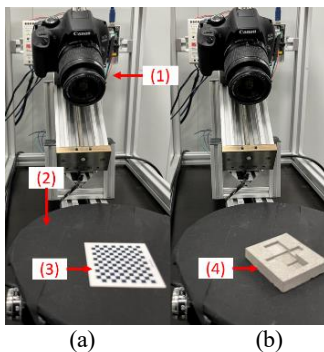


Fig. 1 Overview of the photogrammetry system with calibration step setup in (a) and measurement step setup in (b). (1) camera, (2) motor-driven rotational stage, (3) checkerboard, (4) measurand.

2.2 Measurement pipeline

This section shows the basic experimental workflow from image acquisition to dense point cloud generation (fig. 2) as follows:

- (1). Camera calibration using an accurately calibrated

checkerboard to obtain the camera intrinsic, distortion, and extrinsic parameters from each image-shooting position (each image taken every 6° for a total of 60 images, red circle indicates camera positions).

- (2). Placement of the measurand on the stage and the image acquisition from the same 60 camera positions by step (1), ensuring there are sufficient overlapping areas of the measurand between each image for subsequent image matching.
- (3). Integration of the calibration data and the image set to COLMAP [8] open-source 3D reconstruction program (detail shown in section 2.2).
- (4). Execution of feature extraction, image registration and matching, bundle adjustment and reorientation steps, where the sparse 3D points are then triangulated and refined [9].
- (5). Visualisation of result for sparse point clouds

The sparse point cloud is fed as priori information into two different densification processes to expand the sparse point clouds from thousands to millions of points [9]. The steps (6) and (7) below show the COLMAP MVS operation and steps (8) and (9) explain the 3DGS operation.

- (6). Use of the distortion parameter obtained in step (1) to perform the image undistorted operation on the initial image set and input the obtained result along with the sparse point cloud as priori information into the MVS process.
- (7). Execution of image matching, geometric and depth map generation, point cloud refinement, and stereo fusion steps to generate a dense point cloud [3,9].
- (8). 3DGS definition of Gaussian distribution for each point in the sparse point cloud. This includes the centroid, standard deviation and weights for colour and density. Projection of the 3D Gaussian distribution into 2D space by accumulating multiple Gaussian distributions to form the final image. Finally, 3DGS performs a depth-based optimization [4,5].
- (9). Visualisation of rendering results in the graphical user interface.

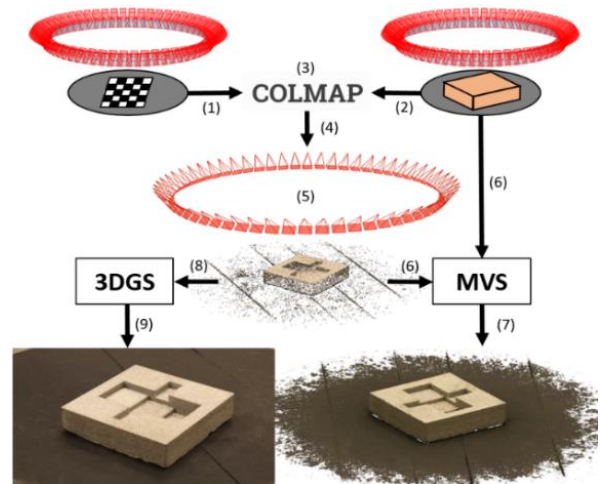


Fig. 2 Overview of dense point cloud reconstruction by 3DGS and MVS.

2.2 Workflow of the COLMAP section

This section shows the detailed workflow of the scale-calibrated

sparse point cloud generation by COLMAP (steps (3) and (4) from fig.2, and summarised in fig.3:

- (1). Camera calibration by using checkerboard, detail shown in section 2.3
- (2). Compute the rotation matrices into quaternion by function (1-5) and generate the files including the calibrated camera intrinsic, extrinsic (quaternions) and distortion data.

$$R = \begin{bmatrix} r_{11} & r_{12} & r_{13} \\ r_{21} & r_{22} & r_{23} \\ r_{31} & r_{32} & r_{33} \end{bmatrix} \quad (1)$$

$$Q_\omega = \frac{1}{2} \sqrt{1 + r_{11} + r_{22} + r_{33}} \quad (2)$$

$$Q_x = \frac{r_{32} - r_{23}}{4Q_\omega} \quad (3)$$

$$Q_y = \frac{r_{13} - r_{31}}{4Q_\omega} \quad (4)$$

$$Q_z = \frac{r_{21} - r_{12}}{4Q_\omega} \quad (5)$$

- (3). Use the image set of measurand fed into the COLMAP without any extra prior information, generate an estimated (uncalibrated) sparse point cloud. Generate the corresponding files including the estimated intrinsic, extrinsic (quaternion) and distortion data.
- (4). Using the plane and origin of the circle formed by the estimated camera pose as the reference, transform the calibrated camera extrinsic from external coordinate system to the COLMAP coordinate system and get the scale factor by normalisation between the two sets of cameras, detail shown in section 2.4.
- (5). Use the calibrated intrinsic and distortion parameters with the extrinsic parameters transformed from step (4) as priori information to feed into COLMAP and obtain the calibrated sparse point cloud, and continue with the remaining steps from section 2.2.

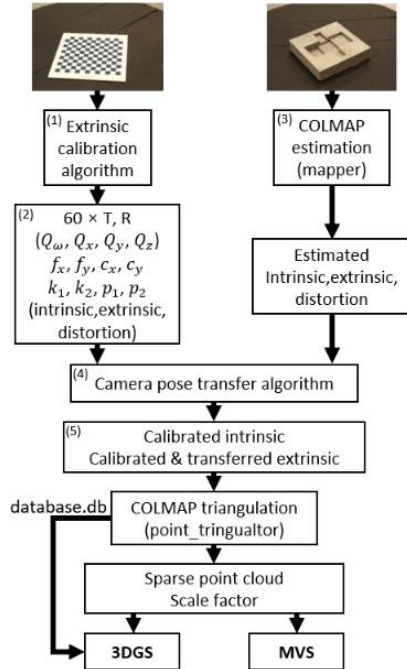


Fig. 3 Scale-calibrated sparse point cloud generation pipeline with COLMAP.

2.3 Extrinsic parameter calibration algorithm

This section is the detailed workflow from step (1) shown in fig.3. This algorithm is designed for processing and analysing the camera extrinsic parameters in a structured environment. The calibration target is a precisely calibrated matte ceramic checkerboard grid with known dimensions of 13×12 , where each cell is a square with a side length of 4 mm, and the number of internal black and white corner points is 132.

Here are the explanations for the three main steps:

Camera calibration:

- Calibrate the intrinsic parameter including focal length (f_x, f_y) and principal point (c_x, c_y), and distortion parameter including radial (k_1, k_2) and tangential (p_1, p_2).
- Calculate the reprojection errors to evaluate the performance of the calibration result (fig.4).

Data structure preparation:

- Define the size of each square on the checkerboard and the number of corner points, use the above information to generate corresponding points in the world coordinate system.
- Load the checkerboard image set and define the image dimension.
- Record the location vectors of the checkerboards detected in each image with the corresponding camera pose (position and orientation).

Image processing:

- Detect the corner point of each image after correcting lens distortion for each image using the intrinsic and distortion parameters. Compute extrinsic parameters including 60 rotation matrices and translation vectors from the image corner points and predefined points in the world coordinate system. Convert these parameters into camera poses (position and orientation).

The illustration of the calibrated camera pose in the world coordinate system are shown in the fig.5

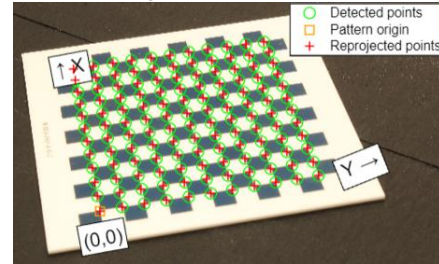


Fig. 4 Detected and reprojected dots from the corner point of checkerboard in the camera calibration step.

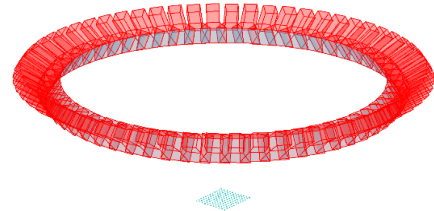


Fig. 5 Total 60 camera poses and predefined points in the world coordinate system.

2.4 Camera pose transfer algorithm

This section is the detailed workflow from step (4) in fig.3. This algorithm is designed to use the camera extrinsic parameter to calculate the camera position and orientation, fit the 3D circle, convert the calibrated camera pose into the coordinate system of the estimated camera pose to achieve data calibration and alignment, and finally output the converted camera pose and scale factor.

The following steps explain the main steps:

- (1). 3D circle fitting to the camera position by two sets of extrinsic parameters (calibrated and estimated), calculating the origin and radius of the enclosed circle, and calculating the scale factor using the radii of the two circles.
- (2). Normalize the circle formed by the calibrated camera pose to be at the same plane and origin as the circle formed by the estimated camera pose. Then, a rigid transformation (rotation and translation) from the calibrated pose to the estimated camera pose is computed.
- (3). Apply the rigid transformation to generate the new rotation matrices and translation vectors for the 60 cameras and convert to quaternions.

2.5 Reference mesh data acquisition

This section shows the reference mesh acquisition of the measurand. The experimental reference was obtained using GOM ATOS Core 300 [10], fig. 6 (a) highlights the hardware setup of the experimental procedure. Fig. 6 (b) merged the meshes from a total of 34 viewpoints with field of view 300 mm × 200 mm. The manufacturer states a probing size error of 0.006 mm, and a sphere spacing error of 0.020 mm. The final fused mesh (fig. 6 (b)) obtained from all viewpoints had a total of 13,055,580 faces.

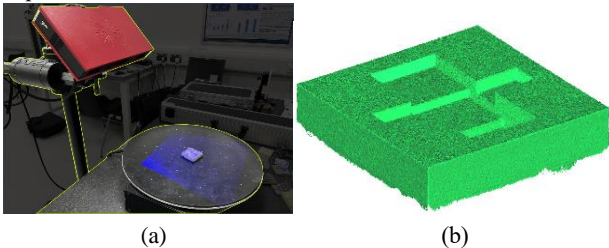


Fig. 6 GOM ATOS FPP system experimental procedure for ground truth mesh acquisition. (a) hardware setup, (b) obtained mesh.

3. Preliminary results and discussion

This section shows the data obtained from each step by the methodology section and the corresponding analysis.

3.1 Point cloud result

Fig.7 shows the scale-calibrated sparse point cloud from COLMAP triangulation process in section 2.2 step (5), this sparse cloud is used as the priori data for the MVS and 3DGS densification process to obtain the scale-calibrated dense point cloud shown in fig.8 (a) and (b) respectively. Table 1 shows the number of points of the initial sparse cloud and the dense clouds after two different densification processes. The point cloud after COLMAP densification is 434.48 times more than the initial sparse cloud, and the dense cloud obtained by 3DGS is 22.58 times more than the initial cloud. Comparing the number of points of the two dense clouds reveals that the COLMAP MVS densification method yields 19.23 times more points than the 3DGS

method.

Table 1 Number of points and standard deviation (SD)

	Sparse point cloud	COLMAP	3DGS
Points	55,864	24,271,575	1,261,660
SD	N/A	0.063	0.618

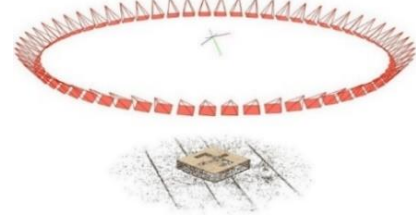


Fig. 7 Scale-calibrated sparse point cloud and calibrated camera poses.

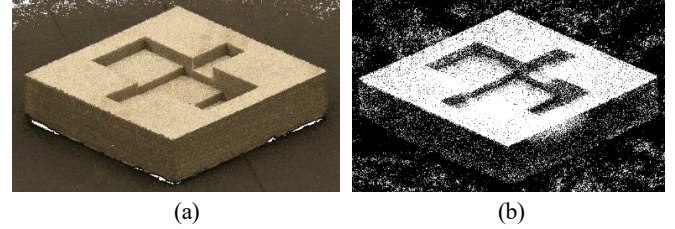


Fig. 8 Scale-calibrated dense point cloud from (a) COLMAP MVS densification, and (b) 3DGS densification.

3.2 Geometric dimensions measurement result

In this section, PolyWorks® [11] is used for the inspection, and the analysis of geometric dimensions and deviations. Using a CAD model with known dimensions as a reference, the point cloud obtained from COLMAP MVS and the mesh obtained from the GOM ATOS are aligned to this CAD model, respectively. By selecting the measurement planes and extracting their features, the deviation from each feature point to the CAD model, the dimension from plane to plane, and the flatness of each plane can be generated. Fig.9 (a) and (b) shows the deviation between each extracted feature points and CAD model by the color bar on the right.

Fig.10 shows the definition of surface flatness, minimum (Min) distance, 3D distance, and maximum (Max) distance within an illustration of two planar cross-section from the measurand. Table 2 shows the measurement results of flatness for each surface selected in fig.9, defining the corresponding surface in the CAD model as reference, and calculating the deviation between the corresponding surfaces in the data obtained from GOM and COLMAP with the CAD model respectively. The surface flatness of the GOM data is closer to zero and the deviation between COLMAP and GOM (as reference) is also calculated. By comparing the measurement results, it can be seen that in the T plane and S1-S3 plane, the deviation of the flatness measurement from GOM and COLMAP is very close, which is all less than 0.035mm. But in the L, R, F, and B planes, the data from GOM is relatively flatter (measured flatness less than 0.1 mm), and the measured flatness of COLMAP data are all greater than 0.22mm.

Table 3 shows the measurement results of the geometric dimensions between the defined surfaces (three different geometric dimensions are defined in fig.10). The geometric dimensions of the GOM and COLMAP data were measured and then the deviation between these data and CAD (reference) was calculated respectively. By comparison, it can be seen that among all the defined dimensions,

regardless of the distance type, the geometric dimension measurement data obtained by GOM is closer to the reference than the COLMAP data. If compared to the data from two sets of measurements with the reference, for the dimensions of F to B and R to L, the Max distance is closer to the reference than the other two distance types; for the dimensions of T to S1, S2 and S3, the Min distance is closer to the reference than the other two distance types. If compare the measurement results from GOM and COLMAP, for the dimensions of F to B and R to L, the Max distance results are the closest than the other two distance types; for the dimensions of T to S1, S2 and S3, the deviations of each distance type are very close. In summary, the mesh data obtained by GOM is more suitable to use as a reference to compare with the point cloud obtained by COLMAP and 3DGS, and COLMAP data gives lower external measurements and higher internal measurements for the geometric dimensions of the measurand.

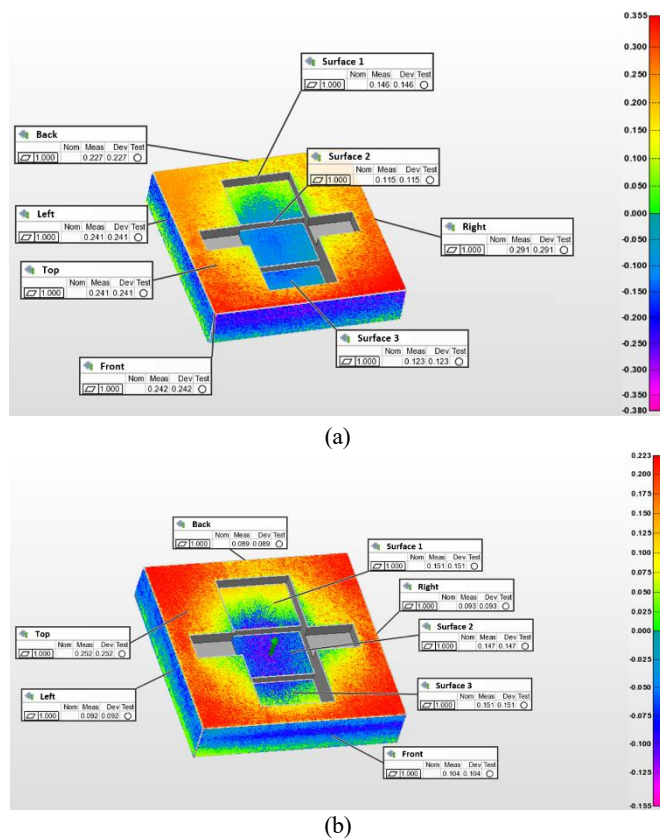


Fig. 9 Surface definition and point-CAD deviation of (a) COLMAP data and (b) GOM ATOS data

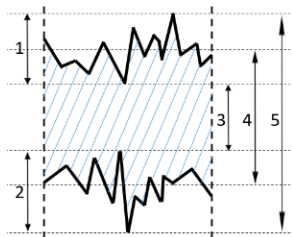


Fig. 10 Illustration of the zoomed-up cross-section of the measurand (1&2. Flatness of two surfaces; 3. Min distance of this cross-section; 4. 3D distance of this cross-section; 5. Max distance of this cross-section)

Table 2 Flatness of the GOM FPP data and COLMAP data (unit: millimetre)

Plane	Measurement GOM	Measurement COLMAP	Deviation
Left (L)	0.092	0.241	0.149
Right (R)	0.093	0.291	0.198
Front (F)	0.104	0.242	0.138
Back (B)	0.089	0.227	0.138
Top (T)	0.252	0.241	-0.011
Surface1 (S1)	0.151	0.146	-0.005
Surface2 (S2)	0.147	0.115	-0.032
Surface3 (S3)	0.151	0.123	-0.028

3.3 Geometric dimensions measurement result

In this section the sparse point obtained from COLMAP and 3DGS were compared with the reference triangular-mesh model obtained from the GOM ATOS instrument. Fig.11 (a) and (b) shows the Gaussian distribution and standard deviation of the point-to-mesh (PTM) distances of these two different reconstructions by CloudCompare [12]. The maximum value of the PTM distance of COLMAP cloud does not exceed 0.323mm, while the maximum PTM distance of 3DGS cloud is 3.100mm, which is 9.597 times more than COLMAP result. Meanwhile, the standard deviation of 3DGS is 9.809 times higher than COLMAP.

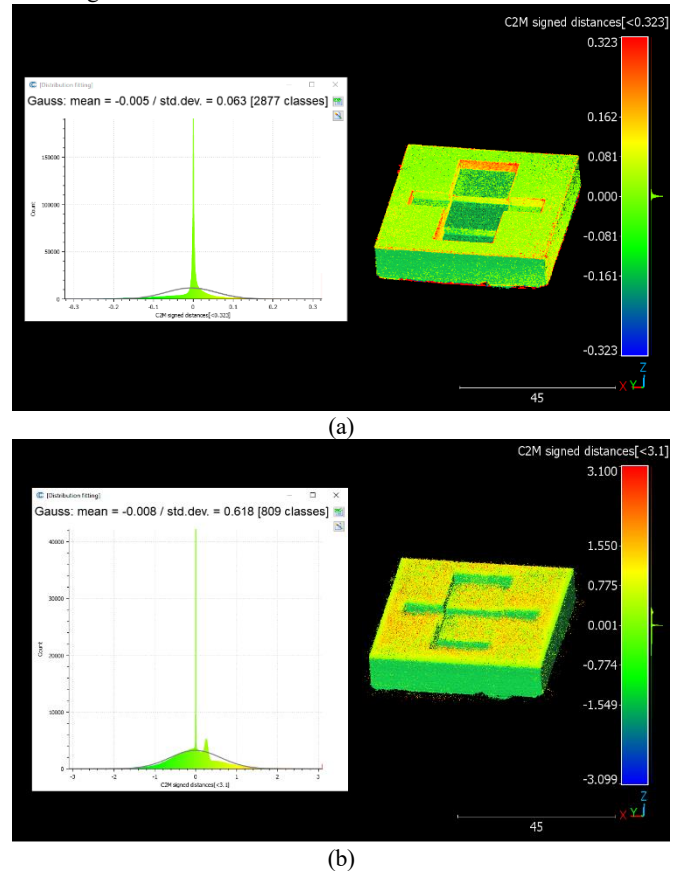


Fig. 11 Comparison of the Gaussian distribution and standard deviation in PTM distances of dense point generated from COLMAP (a) and 3DGS (b).

4. Conclusion and future work

A scale calibrated point cloud generation method from both 3DGS and COLMAP densification operation are presented in this paper. Camera calibration for the positions and originations in the world coordinate system are determined with an accurate calibrated checkerboard. The quality of the reconstructed point cloud is analysed by the comparison with the mesh generated by a commercial industrial FPP instrument. It is shown that the reconstruction from COLMAP MVS densification operation has the lower PTM distance and the closer geometric dimensions when compared to the reference measurement.

The future work is to reduce the standard deviation and PTM distance of the point cloud generated by 3DGS. Each point in the point

cloud generated by 3DGS can be visualised as an ellipsoid in the graphic user interface (GUI), where the more discrete the points in the point cloud are, the larger the volume of the ellipsoid corresponding to the point will be after visualisation. Therefore, the PTM distance and standard deviation of the point cloud can be reduced by limiting the size of the ellipsoid to filter relatively discrete points.

5. Acknowledgment

The authors would like to thank the UKRI Research England Development (RED) Fund for funding this work via the Midlands Centre for Data-Driven Metrology and acknowledge Made Smarter Innovation - Research Centre for Connected Factories (EP/V062123/1) for funding this study.

Table 3 Geometric dimensions of the data from GOM FPP and COLMAP (unit: millimetre)

Dimension type	Distance type	CAD data (ref)	Measurement (GOM)	Deviation (GOM)	Measurement (COLMAP)	Deviation (COLMAP)	Deviation between GOM and COLMAP
Front to Back (plane F to B)	3D	50.000	49.912	-0.088	49.669	-0.331	-0.243
	Min		49.870	-0.130	49.492	-0.508	-0.378
	Max		49.954	-0.046	49.847	-0.153	-0.107
Right to Left (plane R to L)	3D	50.000	49.933	-0.067	49.827	-0.173	-0.106
	Min		49.847	-0.153	49.619	-0.381	-0.228
	Max		50.019	0.019	50.035	0.035	0.016
Top to Surface1 (plane T to S1)	3D	3.000	3.100	0.100	3.157	0.157	0.057
	Min		3.024	0.024	3.078	0.078	0.054
	Max		3.176	0.176	3.235	0.235	0.059
Top to Surface2 (plane T to S2)	3D	5.000	5.169	0.169	5.276	0.276	0.107
	Min		5.153	0.153	5.262	0.262	0.109
	Max		5.184	0.184	5.290	0.290	0.106
Top to Surface3 (plane T to S3)	3D	7.000	7.100	0.100	7.266	0.266	0.166
	Min		7.010	0.010	7.172	0.172	0.162
	Max		7.190	0.190	7.360	0.360	0.170

REFERENCES

- Fraser C and Brown D (1986) Industrial photogrammetry: New developments and recent applications. *The Photogrammetric Record*, 12(68), pp.197-217.
- Sims-Waterhouse D, Piano S, and Leach R (2017) Verification of micro-scale photogrammetry for smooth three-dimensional object measurement. *Meas. Sci. and Tech.*, 28(5), p.055010.
- Do P, Nguyen Q (2019) A review of stereo-photogrammetry method for 3-D reconstruction in computer vision. In 2019 19th International Symposium on Communications and Information Technologies (ISCIT) (pp. 138-143). IEEE.
- Chen G, Wang W (2024) A survey on 3d gaussian splatting. *arXiv preprint arXiv:2401.03890*.
- Kerbl B, Kopanas G, Leimkühler T, Drettakis G (2023) 3d gaussian splatting for real-time radiance field rendering. *ACM Transactions on Graphics*, 42(4), 1-14. International Roadmap for Devices and Systems 2016 Edition. <https://irds.ieee.org/>.
- Eastwood J, Zhang H, Isa M, Sims-Waterhouse D, Leach R, Piano S (2020) Smart photogrammetry for three-dimensional shape measurement. In *Optics and Photonics for Advanced Dimensional Metrology* (Vol. 11352, pp. 43-52). SPIE.
- Isa M, Sims-Waterhouse D, Piano S, Leach R (2020) Volumetric error modelling of a stereo vision system for error correction in photogrammetric three-dimensional coordinate metrology. *Precision Engineering*, 64, 188-199.
- Schonberger J, Frahm J (2016) Structure-from-motion revisited. In *Proceedings of the IEEE conference on computer vision and pattern recognition* (pp. 4104-4113).
- Zhang H, Eastwood J, Isa M, Sims-Waterhouse D, Leach R, Piano S (2021) Optimisation of camera positions for optical coordinate measurement based on visible point analysis. *Precision Engineering*, 67, 178-188.
- <https://www.gom.com/en/products/3d-scanning>
- <https://www.innovmetric.com/products/polyworks-inspector>
- <https://www.cloudcompare.org/>